scientific reports

Check for updates

OPEN

Modulation of the tumor immune microenvironment by Interferon Regulatory Factor 8 enhances immunotherapy in lung adenocarcinoma

Wen Huo[1,4], Minxin Chen[2,4], Cheng Chang[3,4], Jinming Yu[1,2]✉, Dawei Chen[2]✉ & Ruozheng Wang[1]✉

Interferon regulatory factors (IRFs) are integral in governing the expression of Type I interferon (IFN) genes. However, the precise role of IRFs in lung adenocarcinoma remains elusive. Our objective is to elucidate the prognostic implications of IRFs and their potential influence on the immunotherapeutic response in patients with lung adenocarcinoma (LUAD). The association between IRFs expression and clinical as well as prognostic features was evaluated utilizing the TCGA database. Prognostic determinants for LUAD were pinpointed via univariate and multivariate analyses. Nomogram to evaluate prognosis predicated on IRF expression levels. Gene enrichments were conducted to elucidate the mechanisms of action. The degree of immune infiltration was using bioinformatics methods and was validated through a single-cell dataset. We compiled our unique cohort of LUAD patients who underwent anti-PD-1 therapy for subsequent immunohistochemistry and multicolor immunofluorescence staining to gauge the conclusion above. Our findings revealed that IRF8 serves as an independent risk factor for overall survival (OS) in patients with LUAD. An analysis of patients undergoing immunotherapy revealed a positive association between the expression of IRF8 and the response to the treatment. In our specific cohort treated with anti-PD-1, high IRF8 expression was observed to enhance immunotherapy response and prolong OS by modulating immune cell infiltration. Our retrospective analysis suggests that elevated IRF8 expression correlates with improved prognosis in LUAD, with higher IRF8 expression being predictive of a more robust immunotherapy response. Mechanistically, IRF8 expression is associated with a modulated tumor immune microenvironment and improved immunotherapeutic response.

Keywords Interferon regulatory factors, Lung adenocarcinoma, Biological markers, Immune infiltration, Immunotherapeutic response

Based on the CA 2020 Cancer statistics, lung cancer continues to be the second most prevalent cancer, accounting for 11.4% of the total cancer incidence. Furthermore, it is the principal cause of cancer-related mortality, comprising 18.0% of such deaths. The five-year survival rate for lung cancer remains dismally low, approximately 10–20%[1]. With the advent of immunotherapy, this demographic has witnessed considerable therapeutic gains. However, existing data suggests that the objective response rate to anti-PD-1/PD-L1 immunotherapy as a monotherapy in NSCLC is limited to approximately 20%[2]. Numerous studies have delved into the mechanisms underlying immunotherapy, suggesting that factors such as tumor antigen expression and interferon signaling pathways might contribute to resistance towards immunotherapy[3].

[1]Department of Radiation Oncology, Affiliated Tumor Hospital of Xinjiang Medical University, Urumqi 830011, Xinjiang, China. [2]Shandong Provincial Key Laboratory of Precision Oncology, Shandong Cancer Hospital and Institute, Shandong First Medical University and Shandong Academy of Medical Sciences, Jinan 250117, Shandong, China. [3]Nuclear Medicine Department, Affiliated Tumor Hospital of Xinjiang Medical University, Urumqi 830011, Xinjiang, China. [4]Wen Huo, Minxin Chen and Cheng Chang contributedequally to this work and share first authorship. ✉email: sdyujinming@163.com; dave0505@yeah.net; wrz8526@vip.163.com

Interferon regulatory factors (IRFs) are a family of transcription factors comprising nine genes. With the exception of IRF6, all members of this gene family are known to play a role in regulating the IFN response[4]. Specifically, IRF1, IRF3, IRF5, IRF7, and IRF8 are involved in regulating type I IFN responses, which are mediated through Toll-like receptor signaling pathways[5,6], cellular messenger RNA[7], and DNA sensing systems[8]. IRF1 and IRF8 have been identified as key regulators that can induce the production of IFN-γ, the sole member of the type II IFN family, which is crucial for mounting an effective anti-tumor immune response[9]. Additionally, IRF1 and IRF3 may also contribute to the regulation of the type III IFN response[10].

Prior investigations have not comprehensively examined the overall expression levels and functional mechanisms of the IRF gene family in patients with LUAD. The present study aimed to assess the expression profiles of IRF genes in LUAD patients, investigate potential cellular activation mechanisms, and explore their prognostic and therapeutic predictive value. To achieve this, we utilized genomic and clinical data from The TCGA database to analyze the correlation between IRF genes expression and clinical characteristics of LUAD patients. Survival analysis of TCGA data was conducted using KM mapper to generate log-rank *p*-values. Univariate and multifactorial analyses were performed to identify independent prognostic predictor molecules for LUAD. Nomograms were constructed to assess the prognostic and predictive significance of the IRF genes in LUAD. Additionally, we employed the GEO dataset and our own cohort of LUAD patients who underwent immunotherapy to evaluate the impact of IRF genes expressions on the extent of response to immunotherapy. Mechanistically, gene enrichment and immune infiltration analyses were employed to elucidate the potential biological functions of IRF genes in LUAD. Furthermore, multicolor immunofluorescence staining of immunotherapy treated LUAD patients was conducted to validate our analyses and clarify that high expression of IRF8 is positively associated with prognosis and efficacy of immunotherapy in LUAD.

Methods

Data resource

Fragments per kilobase million (FPKM) values for patients with LUAD were acquired from the LUAD datasets of The TCGA (https://portal.gdc.cancer.gov/). Additionally, clinical and pathological attributes, including sex, age, and stage, along with patient prognoses, were obtained from the UCSC Xena database (http://xena.ucsc.edu/). After eliminating samples that lacked complete clinical information, a total of 513 tumors and 59 normal tissue samples were collated, including 57 paired data. Differences in IRF genes expression between normal and tumor tissues were analyzed using R software, with subgroups stratified according to TNM stage, clinical stage, gender, and age. The expression differences based on public data were assessed using the Mann–Whitney U test (Wilcoxon rank-sum test), while paired samples were analyzed using the paired samples t-test. The R package ggplot was utilized for data visualization.

The Kaplan–Meier Plotter Immunotherapy dataset is a comprehensive resource comprising gene expression and clinical data, aimed at identifying biomarkers for responses to anti-PD-1, anti-PD-L1, and anti-CTLA-4 immunotherapies. It utilizes GEO to select datasets that contain both clinical response and transcriptomic data, irrespective of cancer type[11]. Similarly, the ROC Plotter database is derived from pan-cancer immunotherapy data within the GEO database, incorporating clinical treatment details and transcriptomic cohorts. This database facilitates receiver operating characteristic (ROC) analysis for all genes and conducts Mann–Whitney tests between treatment response groups to pinpoint features associated with treatment response[12]. Data from the ICI-treated datasets (GSE93157) were sourced from the GEO database. The GSE93157 dataset comprised 65 patients diagnosed with LUAD, lung squamous cell carcinoma (LUSC), head and neck squamous cell carcinoma (HNSCC), melanoma, and cutaneous melanoma, all of whom had undergone anti-PD-1 immunotherapy (pembrolizumab or nivolumab). After excluding the patients who did not meet the requirements of 2-year PFS follow-up, the remaining 62 cases. Within these datasets, we probed the correlation between the expression of IRF8 and two years progression-free survival (PFS).

Patient tumor samples

A total of 44 tumor biopsy specimens were collected from patients diagnosed with LUAD at Shandong Cancer Hospital between August 2019 and April 2021. Prior to sample collection, these patients had not undergone any antineoplastic therapy, including chemotherapy, radiotherapy, targeted therapy, or immunotherapy. The patients were categorized based on the UICC/AJCC staging system (8th edition). The clinical characteristics and survival data of the IHC cohort were retrospectively recorded. The primary treatment for the patients consisted of radiotherapy or chemotherapy, in addition to anti-PD-1 treatment as first-line therapy. The study received approval from the Medical Ethics Committee of Shandong Cancer Hospital and Research Institute and informed consent was obtained from all subjects, the ethical approval reference number: SDTHEC2023004026. Specific inclusion and exclusion criteria can be found in Supplement Table S1. All methods were performed in accordance with the relevant guidelines and regulations.

The evaluation of curative effects includes both short-term and long-term effects. Short-term efficacy is assessed using the RECIST 1.1 evaluation criteria, where patients with complete response (CR), partial response (PR), or stable disease (SD) are considered favorable, while those with progressive disease (PD) are considered unfavorable. The long-term effect is evaluated based on the 2-year overall survival (OS) rate. Continuous clinical benefit (DCB) after immunotherapy is defined as achieving complete remission, partial remission, or disease stability for more than 6 months, while PD is defined as no sustained benefit (no-DCB).

Survival analysis

The survival analysis in this study utilized The TCGA data, GEO data and IHC-cohort. Specifically, gene expression data (RNA-seq) from the LUAD cohorts were obtained from the UCSC Xena website (http://xena.ucsc.edu/). The protein expression levels were derived from our IHC cohort. Overall survival was set as the clinical

endpoint, and the cutoff value was determined based on the median level of IRF expression, dividing the lesions into two groups. Survival curves were generated using the Kaplan–Meier method and the Survminer software packages. Statistical significance was determined using the log-rank test, with a threshold set at $P < 0.05$.

Furthermore, we examined the association of IRF genes expression with clinical outcomes using the log-rank test, univariable Cox regression modeling, and multivariable Cox regression modeling. To confirm the factors influencing prognostic outcomes and treatment responses, we carried out a multivariate Cox regression analysis. The nomogram included variables such as age, gender, ECOG performance status score, T stage, N stage, M stage, and IRF genes expression. Variables that displayed *P*-values less than 0.10 in the univariate analysis were included for the estimation of prognostic significance. In the multivariate analysis, a P-value of less than 0.05 was deemed statistically significant.

GSEA analysis of IRFs in LUAD

GSEA 4.1.0 software was utilized to investigate the relationships between gene expression subgroups exhibiting high and low IRFs and varying pathways. This analysis was performed using the entire gene expression matrix of the TCGA-LUAD cohort from The Cancer Genome Atlas. For the GSEA, we employed C2.cp.kegg.v7.4.symbols.gmt as our reference gene set, and the phenotype was labeled according to the gene expression level. The normalized enrichment score (NES) was computed by executing gene set permutations 1,000 times. A P-value of less than 0.05 and a false discovery rate (FDR) of less than 0.1 is considered statistically significant.

Tumor immunology analysis

We utilized the TIMER database (https://cistrome.shinyapps.io/timer/) for our immune infiltration analysis. This comprehensive resource allows systematic analysis of immune infiltrates across various cancer types[13]. Specifically, we employed it to examine the associations between IRF genes expression and immune infiltration LUAD. Immune cell types under consideration included B cells, CD8 + T cells, CD4 + T cells, macrophages, neutrophils, and dendritic cells.

In order to quantify the levels of infiltration among these diverse immune cell types, we utilized the single-sample GSEA (ssGSEA) implementation provided by the GSVA R package[14]. To validate the findings from our initial analysis, we turned to the Tumor Immune Single-cell Hub (TISCH) database (http://tisch.compbio.cn/home/)[15]. This resource boasts 79 datasets and a staggering 2,045,746 cell entries, spanning both tumor patients and healthy donors, curated from GEO and ArrayExpress. These datasets contribute to developing single-cell RNA sequencing (scRNA-seq) profiles. All data underwent uniform processing to illuminate the components of the tumor microenvironment (TME) at both individual cell and annotation cluster levels. The TISIDB database (http://cis.hku.hk/TISIDB)[16] was utilized in this study to investigate the association between IRF8 and multiple immune characteristics, including immune inhibitors, immune stimulators, and chemokines. The database integrates a total of 4176 records from 2530 publications, which have reported 988 genes associated with anti-tumor immunity.

IHC and multicolor immunohistochemistry (mIHC) staining

Both IHC and multiplex immunohistochemistry (mIHC) samples were obtained from pre-treatment lung biopsy. Tumor tissues from patients were procured and then fixed in 10% buffered formalin before being embedded in paraffin. The tissue sections were subsequently treated with a primary antibody, specifically anti-IRF8 (18977-1-AP, Proteintech, 1:100 dilution), which was followed by secondary antibody application and staining with diaminobenzidine (DAB, Proteintech). Hematoxylin (Vector Laboratories) was used for counterstaining of cell nuclei.

The quantification process was conducted independently and blindly by at least two individuals. Scoring of staining was carried out in terms of the percentage of stained tumor cells and the intensity of staining, each of which had four levels of scoring: 1 indicating 5%, 2 indicating 5–20%, 3 indicating 21–50%, and 4 indicating 51–100%. Similarly, the staining intensity was graded from 1 to 4, corresponding to no staining, low, moderate, and high intensity, respectively. The IHC scores were computed as the product of the percentage and intensity scores, with the scoring performed under 200 × magnification.

Formalin-fixed paraffin-embedded tissues were sectioned at thickness of 4 μm. Deparaffinization of tissue sections was done through xylenes and rehydration through decreasing graded alcohol. AR6 buffer (Akoya Biosciences) was used for antigen retrieval in a microwave oven. Endogenous peroxidase was inactivated by incubation in 3% H_2O_2 for 10 min. Multiplex immunohistochemistry was performed by several rounds of staining, each including a protein block with 1% BSA followed by primary antibody and corresponding secondary horseradish peroxidase-conjugated antibody against mouse or rabbit immunoglobulins (Akoya Biosciences). The slides were then incubated in different Opal fluorophore (1:100) diluted in 1 × Plus Amplification Diluent (Akoya Biosciences). After tyramide signal amplification and covalent linkage of the individual Opal fluorophores (Akoya Biosciences) to the relevant epitope or epitopes, the primary and secondary antibodies were removed via antigen retrieval as previously mentioned and the next cycle of immunostaining was initiated. For the multiplex immunofluorescence staining, we followed the Opal protocol staining method using various markers. CD8 (ab199016, Abcam, 1:200 dilution) was labeled with Akoya Opal fluorophores 690; CD4 (ab20034, Abcam, 1:100 dilution) with Akoya Opal fluorophores 480; CD68 (ab133357, Abcam, 1:200 dilution) with Akoya Opal fluorophores 520; and IRF8 (18977-1-AP, Proteintech, 1:100 dilution) with Akoya Opal fluorophores 620. Nuclei were labeled with DAPI (1:100, Akoya). Following staining, all sections were cover-slipped using the Anti-Fade Fluorescence Mounting Medium (ab104135, Abcam). Following the completion of chromogenic immunohistochemistry analysis with individual markers, both uniplex and multiplex immunofluorescence staining were performed. The Vectra Polaris Imaging System (Akoya Biosciences) was utilized for multichannel imaging. Cell segmentation was achieved through an algorithm that relied on the presence of nuclear DAPI

staining. The fluorescence staining intensity of each marker cell was assessed, and the fluorescence intensity of previous markers in distinct groups was measured as a quantitative index of mIHC.

Statistical analysis

R software (version 4.2.0) was used for data analysis. For variables following a normal distribution, we employed the independent t-test to calculate the statistical significance. Conversely, for non-normally distributed variables, we used the Mann–Whitney U test to analyze differences between two groups of continuous variables.

For evaluating the statistical significance between two groups of categorical variables, we either used the Chi-square test or Fisher's exact test, depending on the nature of the data. Correlations between different genes were established using Pearson's correlation analysis, from which we obtained the correlation coefficients. For survival analysis, we used the survival package in R. Kaplan–Meier survival curves were constructed to discern differences in survival, and the log-rank test was used to verify significant survival differences between groups. To identify independent prognostic factors, we carried out both univariate and multivariate Cox regression analyses. All statistical *P*-values were considered from a two-sided perspective, and a P-value of less than 0.05 was deemed statistically significant. To assess the impact of different treatment modalities on survival outcomes, we employed Firth's penalized likelihood regression model for multivariate Cox analysis to correct for small sample biases, despite the limited sample sizes in each subgroup. Immunotherapeutic agents (Pembrolizumab, Camrelizumab, Sintilimab, and Tislelizumab) were included as categorical variables in the model, with Tislelizumab serving as the reference group.

Code availability statement

The codes used for the bioinformatics analysis in this article are described in the Methods section and the Supplementary Materials. For further inquiries, please contact the first author or the corresponding author for access.

Results

Expression and mutation patterns of IRF genes in LUAD

In the initial phase of our investigation, we evaluated the expression levels of IRF genes in the transcriptomes of the Cancer Cell Line Encyclopedia (CCLE) and The TCGA databases. In the CCLE database (Supplementary Figure S1), all nine genes of this family were identifiable in over 30 tumor cell types. The Transcripts Per Million (TPM) expression of IRF genes was compared across 35 different types of cancer (as per the TIMER database), and our results indicated that the expression of most IRF genes varied significantly between tumor and normal tissue (Supplementary Figure S2). The TCGA database, comprising 517 lung adenocarcinoma patients, revealed relatively high expression of IRF3/4/6/7/9 (Fig. 1A) and low expression of IRF1/2/8 in tumor tissues when compared to normal lung tissues (Fig. 1C). These findings were corroborated in 57 paired cancer and adjacent non-cancerous tissue groups (Fig. 1B,D).

Further investigation of IRF genes alterations was conducted via cBioPortal, providing deeper insights into the molecular characteristics of IRF family members in lung adenocarcinoma. Alteration frequencies for each gene ranged from 0.8% to 3% (Supplementary Figure S3A). An extensive examination of 3745 samples from 3595 patients across 11 lung adenocarcinoma datasets demonstrated that the overall frequency of alterations in IRF genes varied between 0.99% (6/604) and 20.93% (108/516), with mutations, deep deletions, and amplifications being the most prevalent types of alterations (Supplementary Figure S3B). The three genes with the highest mutation frequencies were IRF6, IRF8, and IRF9. IRF8 predominantly exhibited deep deletion mutations, whereas IRF6 and IRF9 primarily showed amplification mutations. Additionally, we found that patients with IRF gene alterations exhibited a longer overall survival than those without such alterations ($P = 0.013$) (Supplementary Figure S3C).

Moreover, we analyzed differences in IRF genes expression within clinical subgroups categorized by clinical stage, T/N/M stage, gender, and age. Our findings indicated that the expression of IRF4, IRF8, and IRF9 were significantly associated with the clinical stage (Supplementary Fig. 4A). A deeper analysis revealed negative correlations between T stage and the expressions of IRF3, IRF4, IRF5, IRF8 and IRF9 (Supplementary Fig. 4B). We found correlations between N stage and the expression of IRF4, IRF7, IRF8, and IRF9, and a negative correlation between M stage and IRF4 expression (Supplementary Fig. 4C). These findings underscore the important role of IRF genes in both tumorigenesis and progression of LUAD.

Prognostic significance of IRF family in LUAD

Our study utilized Kaplan–Meier survival curves to elucidate the prognostic value of IRFs expression levels in patients diagnosed with LUAD. We discovered that elevated expression levels of IRF4 ($P = 0.001$), IRF8 ($P < 0.001$), and IRF9 ($P = 0.009$) in LUAD patients were significantly correlated with improved OS rates (Fig. 2A).

Following this, we sought to determine whether the IRF gene could serve as an independent prognostic factor for OS. To achieve this, we employed both univariate and multivariate Cox regression analyses using The TCGA dataset. In the univariate analysis, we identified significant correlations between prognosis and the following factors: T stage, N stage, M stage, IRF4, and IRF8 ($P < 0.05$). Consequently, these factors were selected for further analysis. In the subsequent multivariate analysis, IRF8 maintained a robust association with OS (Hazard Ratio = 0.586, $P < 0.001$), as illustrated in Fig. 2B.

A prognostic nomogram was constructed to predict OS in LUAD patients (Fig. 2C). This model was based on 15 independent prognostic factors: T stage, N stage, M stage, gender, smoker status, IRF1, IRF2, IRF3, IRF4, IRF5, IRF6, IRF7, IRF8, and IRF9. This nomogram model utilized R library rms package and enabled predictions of 1, 3, and 5-year survival probabilities. Calibration plots confirmed strong concordance between nomogram

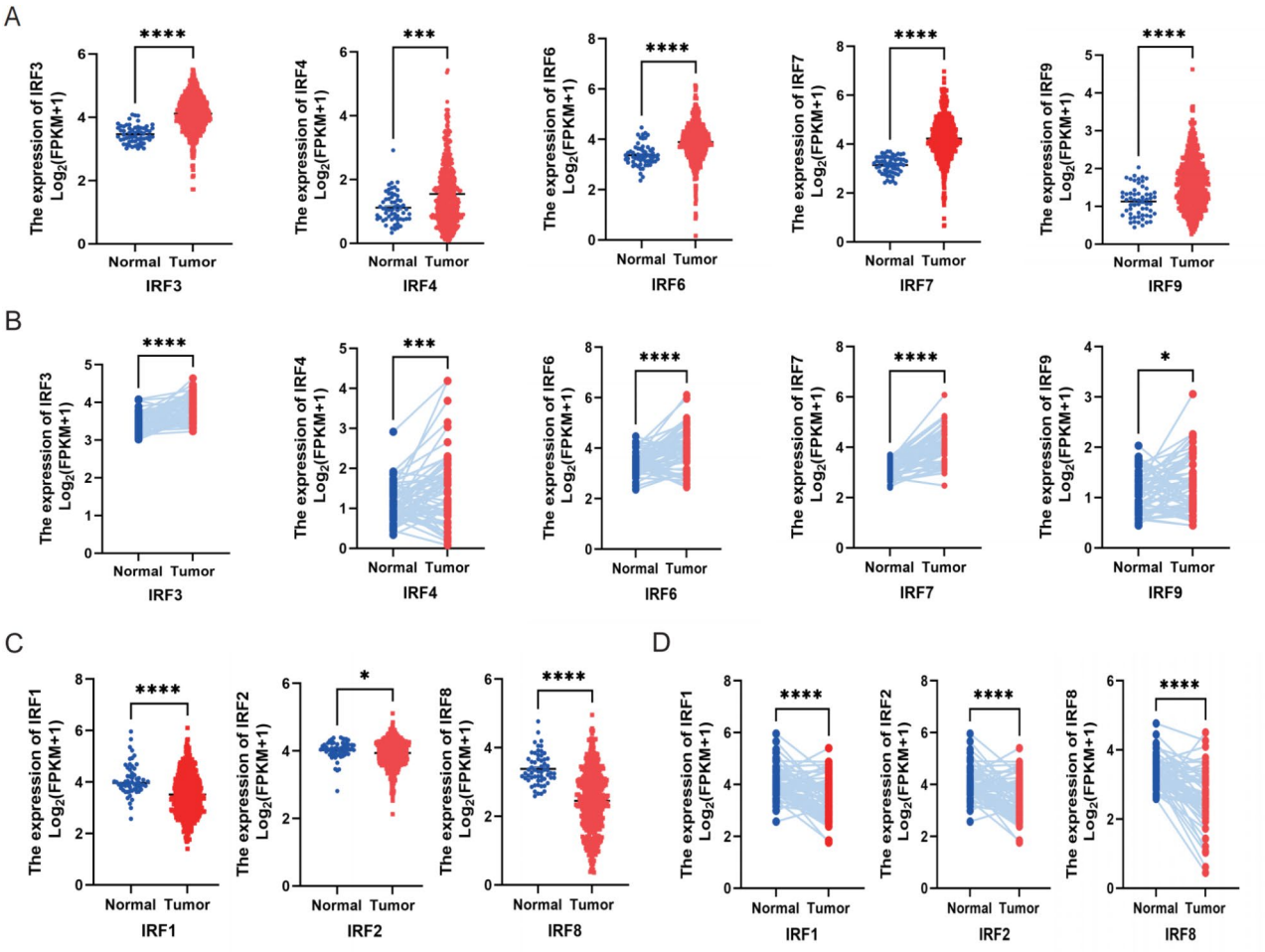

Fig. 1. Differential expression of IRF Family members in LUAD. The expression box plots show that IRF3/4/6/7/9 were upregulated in LUAD tissues, while IRF1/2/8 were downregulated (**A**, **C**). A similar pattern in expression dynamics is observable in a matched sample set comprising 57 pairs of tumor and adjacent non-tumor tissues (**B**, **D**). Statistical comparisons were made using a t-test, ***P-value < 0.001, **P-value < 0.01, *P-value < 0.05. OS was analyzed using the Kaplan–Meier Plotter method, *$P < 0.05$.

predictions and observed outcomes. Internal validation of OS at 1, 3, and 5 years are presented in Fig. 2D. The nomogram exhibited a Concordance C-index of 0.714 (95% CI 0.689–0.739) for OS.

Drawing upon these survival analysis results, IRF8 emerged as a potential independent prognostic factor in LUAD. Intriguingly, we observed under-expression of IRF8 in tumor samples, which was negatively correlated with tumor stage. These findings prompted speculation that IRF8 might serve a beneficial role in LUAD, further emphasizing the need to explore its potential utility in tumor treatment strategies.

Association between IRF8 expression and response to immunotherapy

Our previous findings suggest that IRF8 acts as a favorable prognostic factor in LUAD. Given its role as a type I interferon transcription factor, the potential therapeutic implications of IRF8 in LUAD immunotherapy warrant exploration. Consequently, we proceeded to assess the value of IRF8 in evaluating immunotherapeutic responses.

We initially employed TISIDB to ascertain associations between gene expression and various immune characteristics such as immune inhibitors, immune stimulators, and chemokines. Across all three immune profiles, IRF8 expression demonstrated significant correlations. Among immunosuppressors, IRF8 displayed a notable association with BTLA, HAVCR2, and CD96 (Supplementary Figure S5A). With immunostimulants, a strong correlation was observed between IRF8 and CD28, CD48, CD40LG (Supplementary Figure S5B). Among chemokines, IRF8 was strongly correlated with CCL19, CCL5 and CXCL9 (Supplementary Figure S5C).

We also sought to corroborate the capacity of IRF8 expression to forecast immunotherapeutic benefits. This was done using three different approaches. First, we utilized The Cancer Immunome Atlas (https://tcia.at/), a database based on The TCGA that aims to enhance our understanding of tumor-immune cell interactions. TCIA employs a machine learning approach to identify determinants of immunogenicity and propose an immunophenoscore (IPS), a scoring scheme for solid cancers. We investigated the relationship of IPS between high and low IRF8 expression cohorts. The IPS-PD1/PD-L1/PD-L2, IPS-CTLA4, and IPS-PD1/PD-L1/PD-L2 + CTLA4 were significantly higher in IRF8-high groups (all $P < 0.05$) (Fig. 3A). Considering the relevance of

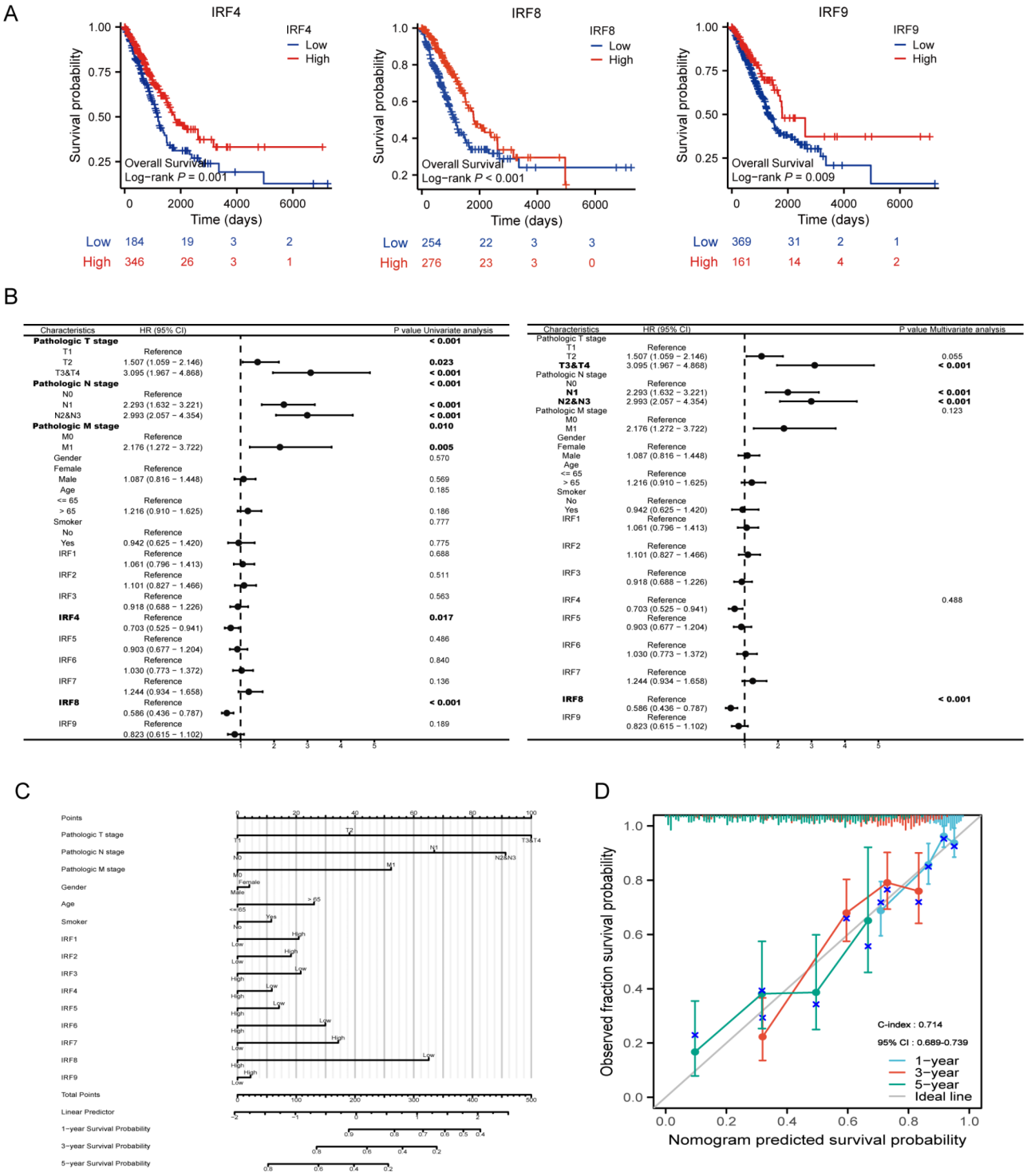

Fig. 2. The prognostic potential of IRF Family members for OS in LUAD. Elevated expression of IRF4, IRF8, and IRF9 correlates significantly with improved patient prognosis (**A**). Univariate analysis reveals a significant correlation between the prognostic value of T stage, N stage, M stage, IRF4, and IRF8 ($P<0.05$). Multivariate analysis further demonstrates that IRF8, exhibiting a hazard ratio of 0.586 ($P<0.001$), is significantly associated with OS ($P<0.05$) (**B**). A constructed nomogram based on 15 independent prognostic factors is employed to predict OS (**C**). The Concordance (C-index) for the OS nomogram was 0.714 (95% CI 0.689–0.739) (**D**).

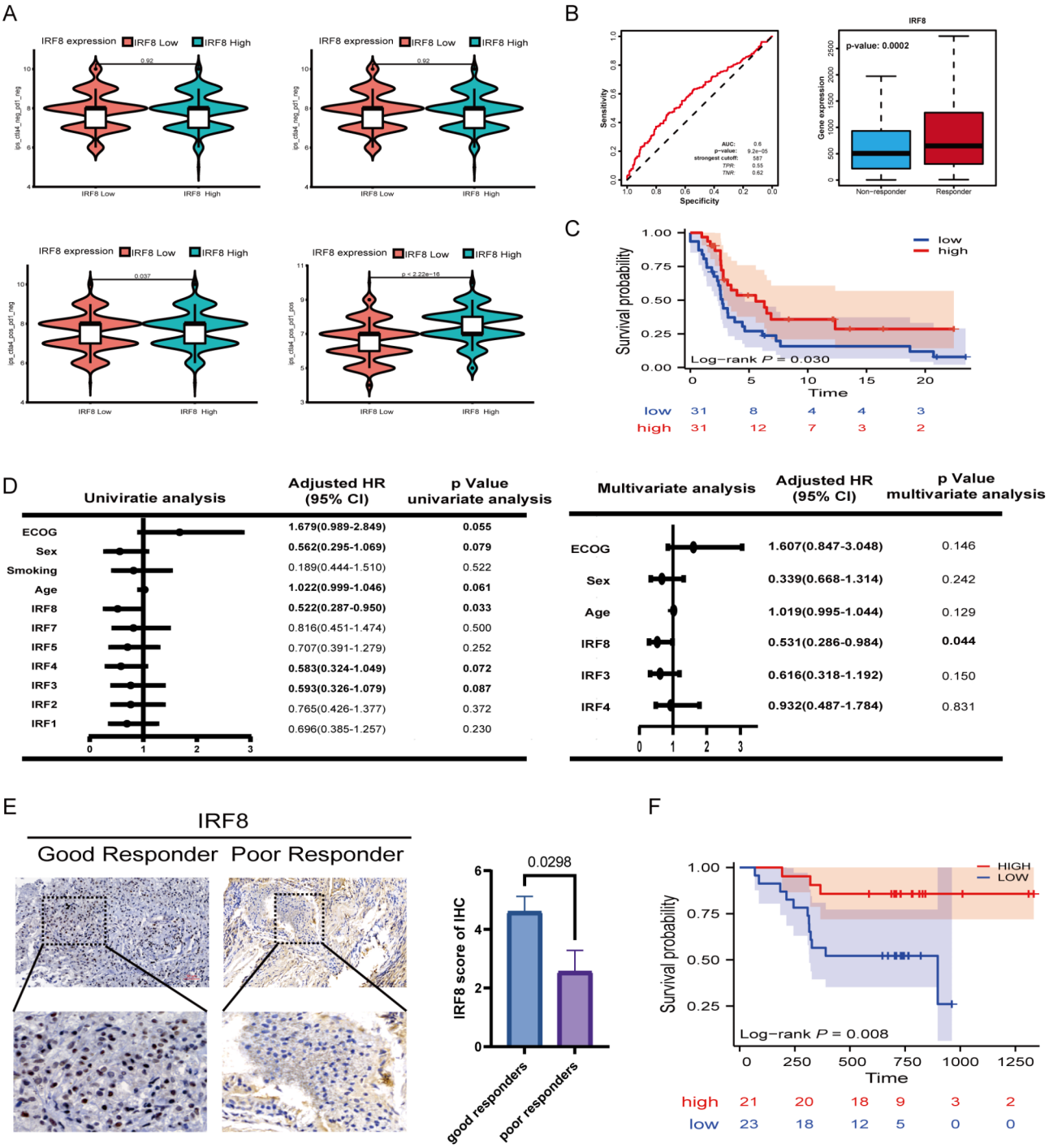

Fig. 3. Association Between Interferon Regulatory Factor Expression and Response to Immunotherapy. The IPS score calculated from the TCIA database was used to predict the correlation between IRF8 expression and response to immunotherapy. The cohort with elevated IRF8 expression had a higher IPS score (**A**). The ROC and boxplot of IRF8 for predicting immunotherapy efficacy (**B**).The cohort of 63 anti-PD- 1-treated patients from GEO database confirmed that increased IRF8 expression was associated with extended PFS (**C**). COX regression analysis identified IRF8 as an independent predictor for PFS (**D**). A cohort of 44 patients with LUAD, treated with anti-PD- 1 at our institution, demonstrated that a higher level of IRF8 expression was observed in the subgroup with favorable to immunotherapy (**E**), and that elevated IRF8 expression was associated with longer OS (**F**).

IPS in immunotherapy, we further assessed the predictive power of IRF8 within the practical immunotherapy application cohorts using the ROC Plotter database. Our findings indicated that the expression level of IRF8 was greater in the anti-PD-1 treatment-responsive cohort compared to the non-responsive one ($P<0.05$) (Fig. 3B). ROC curve analysis revealed an area under the curve (AUC) of 0.6, with $P=9.2e{-}05$, underscoring the statistical significance of this model and suggesting IRF8's potential as a treatment efficacy predictor (Fig. 3C).

To further validate these predictions, multiple datasets were employed for cross-validation. The Kaplan–Meier Plotter Immunotherapy database was used to examine the impact of IRF8 expression on the survival of immunotherapy patients. This resource encompasses data from 520 patients treated with anti-PD-1, 486 with anti-PD-L1, and 121 with anti-CTLA-4 therapies, covering various cancer types. High IRF8 expression significantly correlated with prolonged overall survival (OS) and progression-free survival (PFS) in PD-1 treated cohorts (Supplementary Fig. 6A), a trend also observed in patients receiving PD-L1 (Supplementary Fig. 6B) and CTLA-4 (Supplementary Fig. 6C) therapies. Additionally, the GEO dataset GSE93157 served as an external validation set, containing gene expression and clinical data for 62 patients undergoing anti-PD-1 treatment. Survival analysis based on IRF8 expression indicated a significant improvement in PFS for the high IRF8 expression group ($P=0.03$, Fig. 3C), further supporting the conclusion that IRF8 expression is a viable predictor of immunotherapy efficacy.

Following this, we sought to determine whether the IRF8 could serve as an independent prognostic factor for immunotherapeutic benefits. To achieve this, we employed both univariate and multivariate Cox regression analyses using the GEO dataset. In the univariate analysis, we identified significant correlations between prognosis and the following factors: ECOG, sex, age, IRF8, IRF4, IRF3 ($P<0.1$). Consequently, these factors were selected for further analysis. In the subsequent multivariate analysis, IRF8 maintained a robust association with PFS (Hazard Ratio = 0.531, $P=0.044$), as illustrated in Fig. 3D.

Furthermore, we analyzed the association between IRF8 expression and immunotherapy response in LUAD patients from our IHC cohort. This cohort consisted of 44 LUAD patients who received anti-PD1 therapy (Table 1). There was no significant correlation between IRF8 and the distribution of various clinical characteristics including age, sex, smoking history, ECOG PS score,clinical stage,T stage, N stage, M stage and EGFR mutation in our IHC-cohort LUAD patients ($P>0.05$) (Table 2). We found that higher IRF8 expression was observed in the group with a favorable response ($P=0.0298$, Fig. 3E) and was associated with extended survival ($P=0.008$, Fig. 3F).Multivariate Cox regression analysis revealed that high expression of IRF8 (HR = 0.60, $P=0.03$) and treatment with Pembrolizumab (HR = 0.55, $P=0.02$) were independently associated with improved overall survival (OS). Conversely, Stage IV disease (HR = 1.90, $P=0.006$), elevated ECOG performance status (HR = 1.25, $P=0.03$), and brain radiation therapy (HR = 1.50, $P=0.03$) were identified as significant risk factors (Supplementary Table S7).

Despite the limited sample size of our center's cohort (n = 44), the predictive validity of IRF8 remains consistent across multiple datasets, as evidenced by the independent validation using public databases such as TCGA and GEO. This consistency suggests the potential universality of IRF8 as a predictive marker. Collectively, these findings suggest that IRF8 holds promising potential as a prognostic indicator and a predictor of immunotherapeutic benefits in LUAD.

Functional enrichment and pathway analysis of IRF8 in lung adenocarcinoma in LUAD

As part of a family of transcription factors, IRF8 are likely to function by influencing the transcription of downstream molecules. Hence, we divided samples into groups based on IRF8 expression levels, identified differentially expressed genes, and performed GO and GSEA on these genes to uncover potential mechanisms of action. We first extracted gene expression data from LUAD patients in the TCGA database and stratified them based on IRF8 expression levels, employing a 50% cutoff. A volcano plot was constructed for the differentially expressed genes between the two groups. Protein-coding genes with LogFC ≥ 1.5 and $P<0.05$ were identified as differential genes. From this analysis, we discerned 327 differentially expressed genes across the IRF8 expression groups, with 192 downregulated and 135 upregulated. The top five protein-coding genes among the upregulated genes were H4C6, H1-1, H2BC3, H4C13, and IFNK, and the top five downregulated genes were VGLL2, MAGEA10, ERVH48-1, MAGEA1, TAF11L11 (Fig. 4A, Supplementary Table S2).

Additionally, GO enrichment analysis performed on the differentially expressed genes revealed that the main pathways positively regulated by IRF8 include leukocyte cell–cell adhesion, leukocyte mediated immunity, regulation of T cell activation, regulation of leukocyte cell–cell adhesion, lymphocyte differentiation, and immune response – regulating signaling pathway. Conversely, the pathways negatively regulated by IRF8 include the neuropeptide signaling pathway, hormone activity, alditol: NADP + 1–oxidoreductase activity, negative regulation of blood coagulation, negative hemostasis regulation, and sympathetic nervous system development (Fig. 4C). Moreover, GSEA prediction based on the NES showed the most significantly enriched pathways in samples with high or low IRF8 gene expression. Cytokine-cytokine receptor interaction, chemokine signaling pathway, cell adhesion molecules, JAK-STAT signaling pathway, and natural killer cell-mediated cytotoxicity were the top five pathways enriched in the high IRF8 expression subgroup (Fig. 4B). Conversely, the IRF8 low-expression subgroup showed the highest enrichment in nitrogen metabolism, phenylalanine metabolism, base excision repair, glycine, serine, threonine metabolism, and the citrate cycle (Fig. 4D).

In conclusion, these results suggest that IRF8 primarily regulates the anti-tumor response by modulating the immune system and metabolic pathways.

Associations between IRF8 and TME diversity in LUAD

Our previous results indicated that IRF8 chiefly acts by regulating immune-related pathways. However, its role in modulating the TME remains to be fully elucidated. Therefore, we extended our analysis to explore the relationship between gene expression and the TME.

Characteristic	All patients (n = 44)
Age, n (%)	
Mean ± SD, years	61.34 ± 11.05
≥ 60y	22 (50.00%)
< 60y	22 (50.00%)
Sex, n (%)	
Male	34 (77.27%)
Female	10 (22.73%)
Smoking history, n (%)	
Never	19 (43.18%)
Ever	25 (56.82%)
ECOG PS, n (%)	
0	23 (52.27%)
1	21 (47.73%)
Clinical stage, n (%)	
II	1 (2.27%)
III	13 (29.55%)
IV	30 (68.18%)
T stage, n (%)	
T1	6 (13.64%)
T2	16 (36.36%)
T3	12 (27.27%)
T4	10 (22.73%)
N stage, n (%)	
N0	6 (13.64%)
N1	6 (13.64%)
N2	22 (50.00%)
N3	10 (22.72)
M stage, n (%)	
M0	14 (31.82%)
M1	30 (68.18%)
EGFR, n (%)	
MUT	4 (9.09%)
WT	39 (88.64%)
N	1 (2.27%)
ALK, n (%)	
MUT	1 (2.27%)
WT	42 (95.46%)
N	1 (2.27%)
Chemotherapy, n (%)	
Pemetrexed + Platinum (PP)	21 (47.72%)
Paclitaxel + Cisplatin (TP)	21 (47.72%)
None	2 (4.56%)
Radiotherapy, n (%)	
Lungs	5 (11.36%)
Brain	3 (6.82%)
Bone	4 (9.10%)
None	32 (72.72%)
Immunotherapy, n (%)	
Pembrolizumab	5 (11.36%)
Camrelizumab	8 (18.18%)
Sintilimab	18 (40.91%)
Tislelizumab	13 (29.55%)
IRF8 IHC score, n (%)	
IRF8 high	21 (47.73%)
IRF8 low	23 (52.27%)

Table 1. Clinical characteristics of LUAD patients.

Characteristics	IRF8 low (N = 23)	IRF8 high (N = 21)	Total (N = 44)	*P* value
Age, n (%)				1.00
≥ 60	12 (52.17%)	10 (47.62%)	22 (50.00%)	
< 60	11 (47.83%)	11 (52.38%)	22 (50.00%)	
Sex, n (%)				0.10
Female	8 (34.78%)	2 (9.52%)	10 (22.73%)	
Male	15 (65.22%)	19 (90.48%)	34 (77.27%)	
Smoking history, n (%)				0.12
Never	13 (56.52%)	6 (28.57%)	19 (43.18%)	
Ever	10 (43.48%)	15 (71.43%)	25 (56.82%)	
ECOG PS, n (%)				0.77
0	13 (56.52%)	10 (47.62%)	23 (52.27%)	
1	10 (43.48%)	11 (52.38%)	21 (47.73%)	
Clinical Stage				0.24
Stage II	0 (0.00%)	1 (4.76%)	1 (2.27%)	
Stage III	6 (26.09%)	7 (33.33%)	13 (29.55%)	
Stage IV	17 (73.91%)	13 (61.91%)	30 (68.18%)	
T stage, n (%)				0.60
T1	4 (17.40%)	2 (9.52%)	6 (13.64%)	
T2	7 (30.43%)	9 (42.86%)	16 (36.36%)	
T3	7 (30.43%)	5 (23.81%)	12 (27.27%)	
T4	5 (21.74%)	5 (23.81%)	10 (22.73%)	
N stage, n (%)				0.07
N0	2 (8.70%)	4 (19.05%)	6 (13.64%)	
N1	4 (17.39%)	2 (9.52%)	6 (13.64%)	
N2	9 (39.13%)	13 (61.91%)	22 (50.00%)	
N3	8 (34.78%)	2 (9.52%)	10 (22.72%)	
M stage, n (%)				0.47
M0	6 (26.09%)	8 (38.10%)	14 (31.82%)	
M1	17 (73.91%)	13 (61.90%)	30 (68.18%)	
EGFR, n (%)				0.63
MUT	2 (8.70%)	2 (9.52%)	4 (9.09%)	
WT	20 (86.96%)	19 (90.48%)	39 (88.64%)	
N	1 (4.34%)	0 (0.00%)	1 (2.27%)	
ALK, n (%)				1.00
MUT	1 (4.34%)	0 (0.00%)	1 (2.27%)	
WT	21 (91.32%)	21 (100.00%)	42(95.45%)	
N	1 (4.34%)	0 (0.00%)	1(2.27%)	
Chemotherapy, n (%)				1.00
Pemetrexed + Platinum (PP)	11 (47.83%)	10 (47.62%)	21 (47.73%)	
Paclitaxel + Cisplatin (TP)	11 (47.83%)	10 (47.62%)	21 (47.73%)	
None	1 (4.34%)	1 (4.76%)	2 (4.55%)	
Radiotherapy, n (%)				0.90
Lungs	2 (8.70%)	3 (14.29%)	5 (11.36%)	
Brain	2 (8.70%)	1 (4.76%)	3 (6.82%)	
Bone	3 (13.04%)	1 (4.76%)	4 (9.09%)	
None	16 (69.56%)	16 (76.19%)	32 (72.73%)	
Immunotherapy, n (%)				0.38
Pembrolizumab	3 (13.05%)	2 (9.52%)	5 (11.36%)	
Camrelizumab	6 (26.09%)	2 (9.52%)	8 (18.18%)	
Sintilimab	7 (30.43%)	11 (52.38%)	18 (40.91%)	
Tislelizumab	7 (30.43%)	6 (28.58%)	13 (29.55%)	

Table 2. Clinical characteristics of LUAD patients with IRF8 high and low expression.

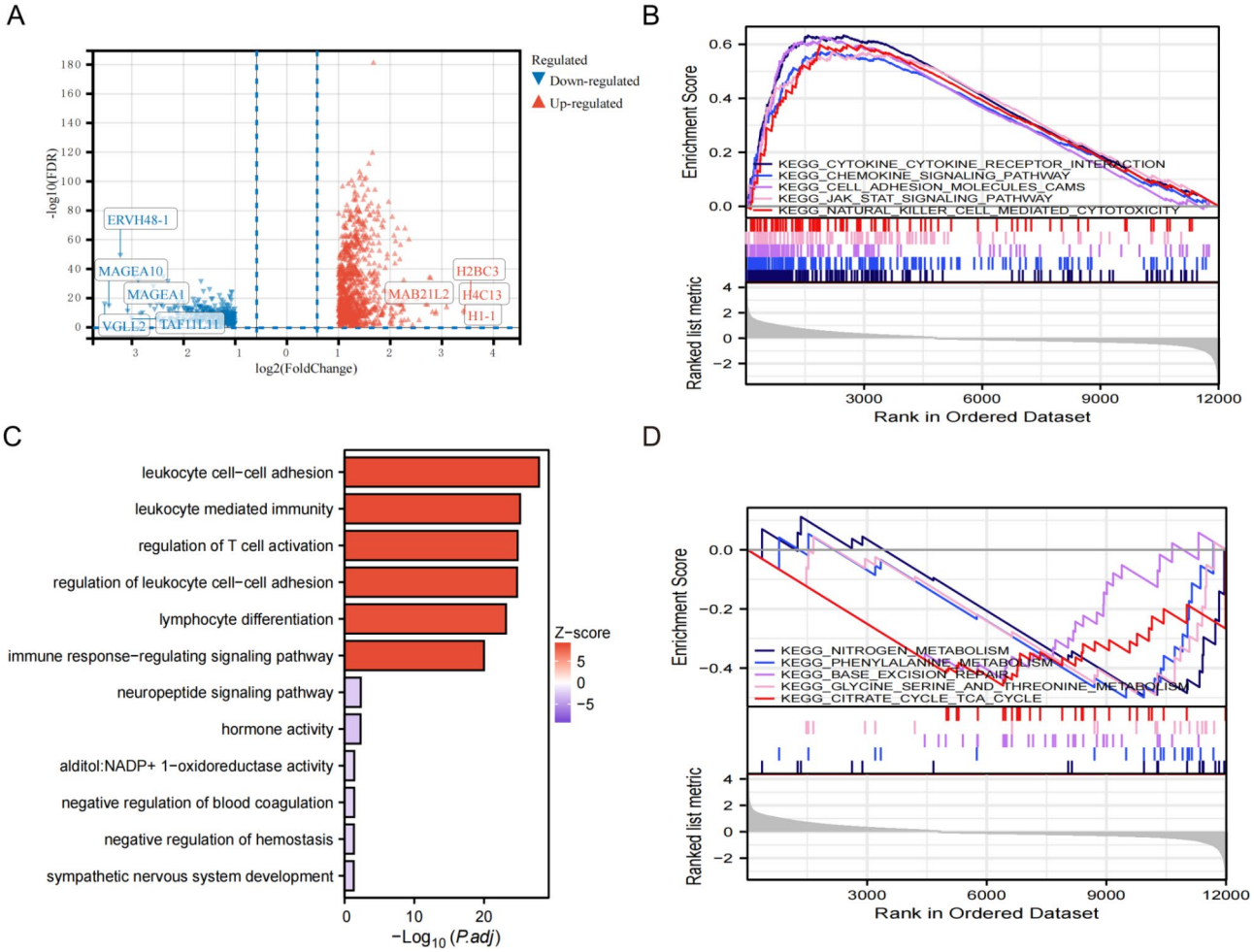

Fig. 4. GO and GSEA enrichment analysis of differentially expressed IRF8. Analysis demonstrated 327 differentially expressed genes in groups of different IRF8 expressions, with 192 genes downregulated and 135 genes upregulated (**A**). The main positively and negatively regulated pathways identified by GO enrichment analysis for genes differentially expressed in response to IRF8 (**C**)**.** The most frequently significantly enriched pathways were predicted in relation to IRF8 expression measured by normalized enrichment score (NES) using GSEA (**B**, **D**). The criteria for identifying differential genes were set for protein-coding genes (Log FC ≥ 1.5, and $P < 0.05$).

First, we assessed the correlation between gene expression and tumor-infiltrating immune cells using the TIMER database. IRF8 exhibited a robust positive correlation with B cells, CD8 + T cells, CD4 + T cells, macrophages, neutrophils, and dendritic cells (DCs) (Fig. 5A). Subsequently, the Estimation of Stromal and Immune cells in Malignant Tumors using Expression data (EPIC) score was applied to quantify the infiltration score of six different types of immune cells. The results showed that higher IRF8 expression was associated with increased infiltration of B cells, CD8 + T cells, CD4 + T cells, neutrophils, and DCs (Fig. 5B). Finally, we validated these findings using the single-cell database TISCH. We selected datasets GSE131907 and GSE139555, which comprise 44 primary/metastatic and 6 primary tumors, respectively (Fig. 5C, Supplementary Fig. 8). We found that IRF8 was highly expressed in B cells, DCs, macrophages, and T cells, and notably, it was rarely expressed in stromal cells (Fig. 5D). These results consistently suggest that IRF8 indeed affects the infiltration of immune cells.

To validate these predicted outcomes, we collected samples from eight patients undergoing anti-PD-1 therapy for mIHC analysis. To eliminate the effects of post-treatment on the immune microenvironment, mIHC staining was performed on pre-treatment lung biopsy tissues from these patients. Our aim was to further investigate the specific ways through which IRF8 influences the effectiveness of immunotherapy. Prior to conducting the mIHC staining, we performed panCK staining on all slices in our cohort. This allowed us to differentiate the tumor area from the stromal area. Subsequently, we used consecutive slices to investigate the relationship between IRF8 and CD4, CD8, and CD68. We utilized different color labels: blue for the nucleus, pink for IRF8, cyan for CD4 + , red for CD8 + , and green for CD68 + . The cohort included four cases with a durable clinical benefit (DCB) (Fig. 6A) and four cases with a non-durable clinical benefit (Fig. 6B). According to the mIHC results, the IRF8 expression levels were higher in the DCB group ($P = 0.0298$) and were associated with an increase in CD4 + and CD8 + T

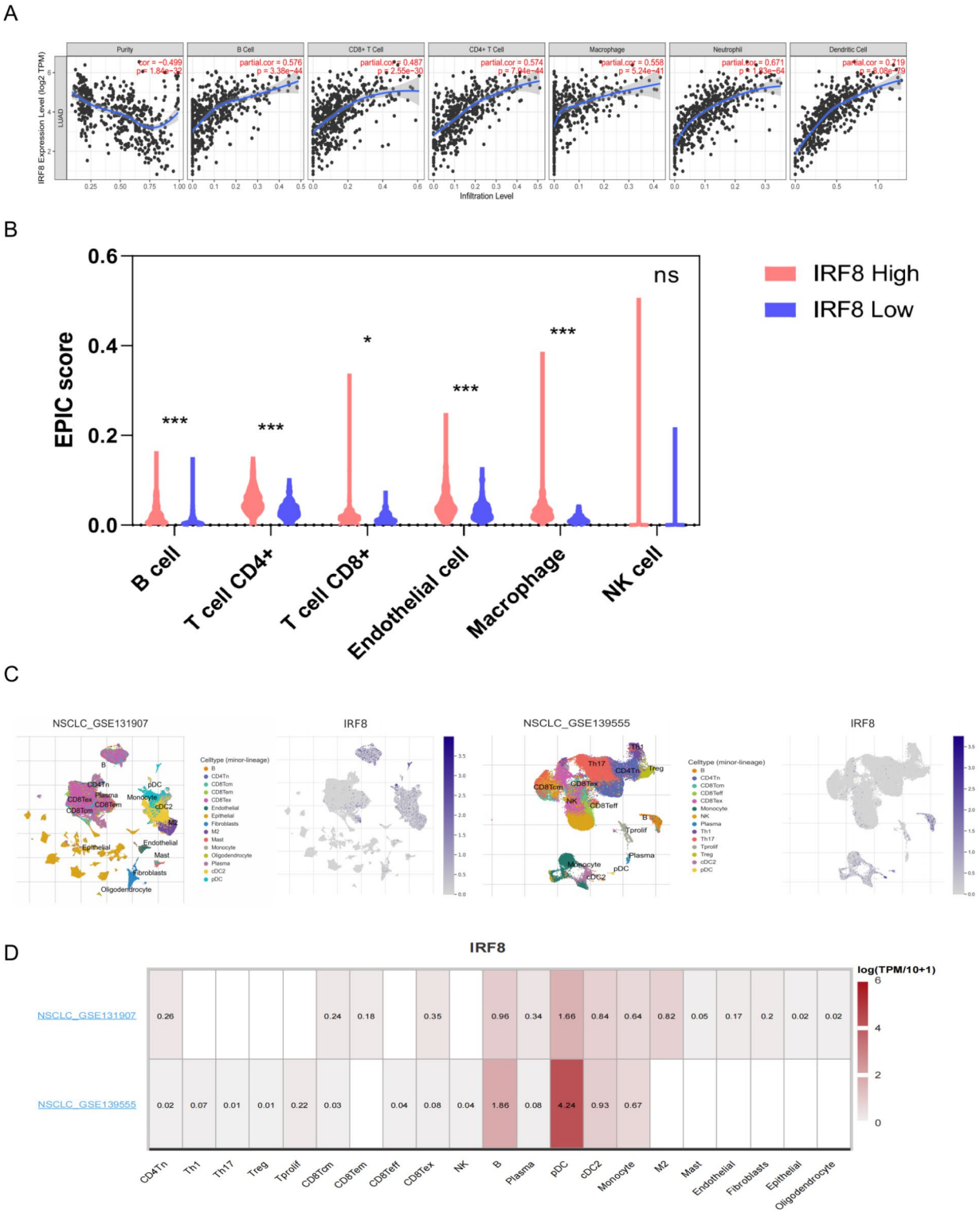

Fig. 5. Correlation of IRF8 expression with immune cell infiltration in LUAD. The scatter plots identify different profiles of immune cells in relation to IRF8 (**A**). EPIC score was used to calculate the infiltration score of 6 different types of immune cells (**B**). The expression level of IRF8 in various TME-related cells was determined by single-cell sequencing data (**C**, **D**).

cell infiltration. Conversely, in the non-responder group, the expression levels of IRF8 were lower and were associated with increased macrophage infiltration (Fig. 6C).

These findings suggest that high levels of IRF8 expression could enhance the efficacy of immunotherapy, possibly achieved through the regulation of immune cell functions in the TME.

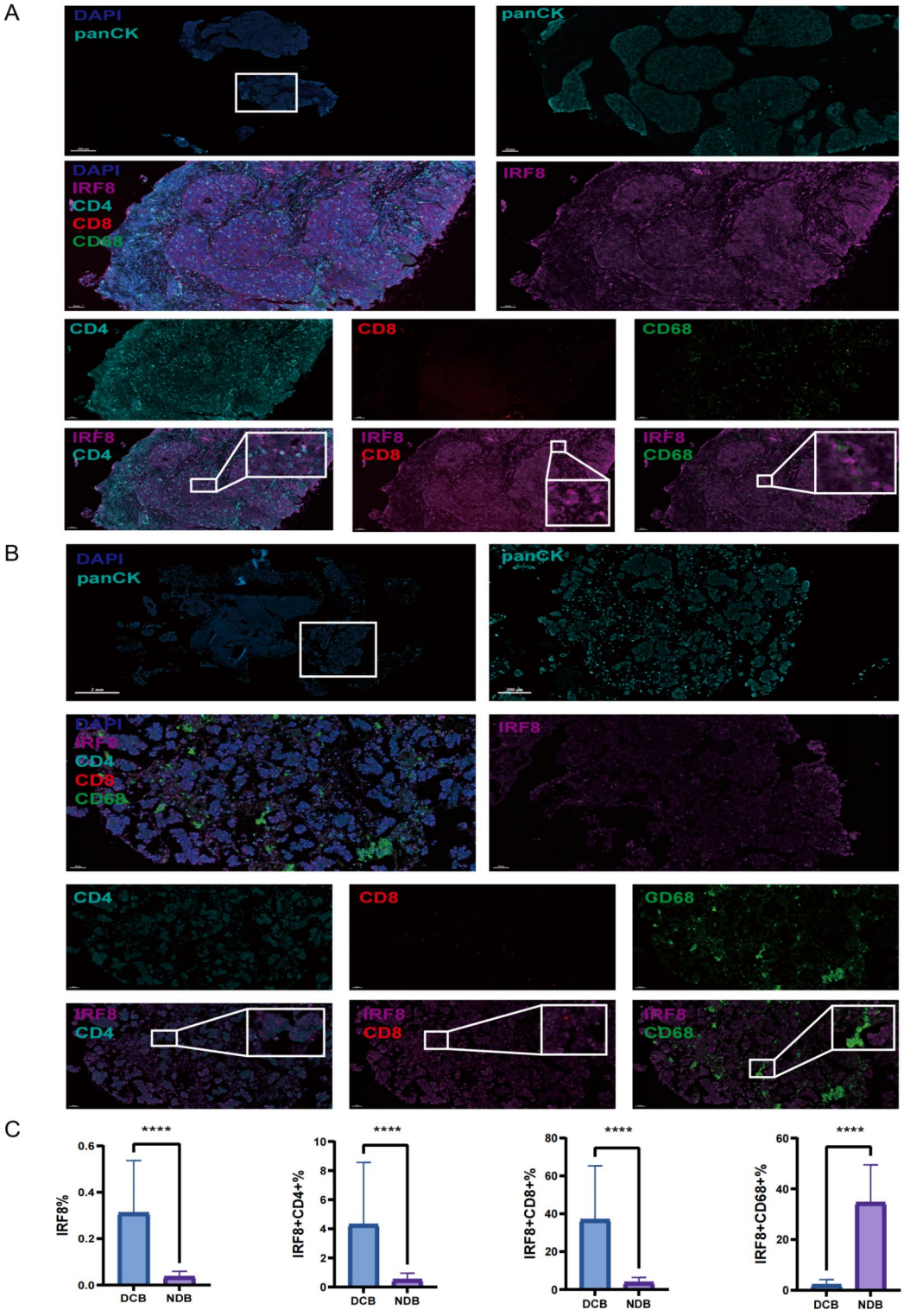

Fig. 6. Association of high IRF8 expression with immunotherapy benefits and immune cell infiltration. Multicolor immunofluorescence shows a higher expression of IRF8 in the cohort with sustained benefits (**A**, **B**). High IRF8 expression correlated positively with CD4 + and CD8 + T-cell infiltration and negatively with macrophage infiltration (**C**).

Discussions

In the treatment of non-small cell lung cancer (NSCLC), anti-PD-1/PD-L1 immune checkpoint inhibitors (ICIs) are extensively utilized for first-line[17,18], maintenance[19], and second-line therapies. Despite the considerable efficacy of immunotherapy, the development of treatment resistance indicates a substantial opportunity for

enhancing overall effectiveness[20]. Consequently, identifying targets that can predict resistance to ICI therapy, as well as accurately determining the patient that would benefit most from treatment, are pivotal areas of ongoing research. Type I interferon plays a critical role in ICIs, with evidence indicating that the effectiveness of PD-1 blockade in various cancers is intimately linked to the activation level of the IFN pathway[21,22]. For instance, mutations in IFNGR1/2 and JAK2 have been identified in non-responders to Ibritumomab therapy[23]. Since the expression of IFN-related genes is regulated by interferon regulatory factors (IRFs), this underscores the potential significance of the IRF family in enhancing immunotherapeutic outcomes.

This study is the first to thoroughly assess the expression of IRF genes and their prognostic significance in lung adenocarcinoma (LUAD). Our analysis of nine IRF genes revealed that IRF8 serves as an independent prognostic marker for LUAD, where it is generally low-expressed. Higher IRF8 expression correlates with improved patient prognosis. Mutation analysis indicated a high mutation rate in the IRF8, predominantly characterized by deep deletions, explaining its reduced expression[24]. Our retrospective analysis revealed that elevated IRF8 expression is associated with prolonged progression-free survival (PFS) and overall survival (OS) in LUAD patients receiving first-line PD-1 therapy. Responders to immunotherapy exhibit higher IRF8 expression. Gene enrichment analysis showed that up-regulated IRF8 expression is associated with immune-related pathways, while down-regulation mainly involves metabolism-related pathways. Additionally, IRF8 expression positively correlates with the infiltration levels of B cells, T cells, dendritic cells, and macrophages in the immune microenvironment. Multiplex immunohistochemistry (mIHC) staining of eight LUAD patients treated with PD-1 therapy revealed that patients with sustained immunotherapy benefits displayed elevated IRF8 levels. This increase in IRF8 expression was associated with co-expression of CD4 + and CD8 + T cells, whereas macrophage expression showed an inverse relationship. In exploratory multivariate analysis, Pembrolizumab treatment showed a numerical trend toward improved survival compared to other PD-1 inhibitors. However, the small subgroup size limits the interpretability of this finding, and further validation in prospective cohorts is required to assess potential inter-agent differences. Although this result should be interpreted with caution due to the limited sample size in the Pembrolizumab group (only 5 cases), it nonetheless indicates a potential association with the drug's specific mechanisms (such as differences in Fc structure or dosing schedules). Future prospective studies are needed to validate the efficacy heterogeneity among different PD-1 agents and to further investigate the application value of IRF8 as a stratification factor in various immunotherapy contexts.

As a member of the IRF family, IRF8 is involved in various physiological and pathological processes[9,25]. Given the correlation between PD-1 blockade efficacy and IFN pathway activation, and considering that IRF8 is a Type I interferon transcription factor, it may significantly impact immunotherapy outcomes. Previous research indicates that IRF8 enhances immune cell activation, modulates immunosuppressive factors, and inhibits tumor progression[26,27]. It typically forms heterodimers with IRF1 and is induced by IFN and lipopolysaccharides in macrophages, collaboratively promoting transcription of macrophage functional genes[28,29]. Studies in hepatocellular and breast cancers have shown a positive correlation between IRF8 expression, prognosis, and anti-tumor therapy response[30,31]. In diffuse large B-cell lymphoma (DLBCL), missense mutations in IRF8 result in a loss of protein function, impair downstream antigen presentation factor expression, and facilitate tumor immune evasion[32]. This mechanism parallels our findings in LUAD, underscoring the critical role of IRF8 in tumor immune regulation.

IRF8 acts as a bridge between innate and adaptive immunity within the immune microenvironment. Research has shown that IRF8 is highly expressed in progenitor and mature cells of the B-cell, cDC1, and pDC lineages and is essential for the development of monocytes and dendritic cells (DCs)[33,34]. Evidence suggests that T cell-mediated tumor regression and response to immune checkpoint blockade (ICB) in various cancers require type 1 conventional dendritic cells (cDC1)[35,36]. Given IRF8's significant impact on cDC1 development[37], it likely affects the tumor microenvironment by regulating immune cell development and infiltration, thereby influencing tumor growth and immunotherapy outcomes. Conversely, downregulation of IRF8 primarily affects metabolism-related pathways such as NADP + 1-oxidoreductase activity, glycine, serine, and threonine metabolism, and the citric acid cycle. Metabolic reprogramming plays a major role in cancer immune evasion. For example, most cancer cells depend on aerobic glycolysis, while oxidative phosphorylation dominates tumor metabolism[38]. Compounds like glutathione are closely linked to immune cell activation[39]. These findings suggest that IRF8 expression correlates with tumor progression and immune evasion phenotypes, potentially mediated through metabolic pathway alterations.

In various cancer types, IRF8 demonstrates potential as a biomarker. In T-cell acute lymphoblastic leukemia (T-ALL), IRF8 silencing correlates with disease progression[40]. In triple-negative breast cancer (TNBC), IRF8 is a key feature of the low-immune subtype, linked to reduced immune infiltration and poor prognosis[41]. In locally advanced rectal cancer (LARC), high IRF8 expression prior to preoperative chemoradiotherapy (CRT) is associated with significant tumor regression and longer disease-specific survival[42]. These findings suggest that IRF8 is closely related to disease progression, prognosis, and treatment response across different cancers. This supports the conclusion that IRF8 may serve as a biomarker for predicting treatment response and survival, providing a foundation for optimizing clinical management.

Based on bioinformatics and multicolor immunofluorescence analyses, we have confirmed that IRF8 influences the tumor immune infiltration environment. IRF8 appears to have a positive prognostic significance for anti-PD-1 treatment in LUAD, likely due to its high expression in innate immune cells that activate the anti-tumor response of immune checkpoint inhibitors. Conversely, low or absent IRF8 expressions may indicate poor immunotherapy efficacy and an increased risk of immune escape. This has been corroborated in B-cell lymphoma, where IRF8 mutation status can assess patient response to CAR19 immunotherapy[43]. In B-cell lymphoma IRF8 mutations can lead to tumor immune escape, suggesting greater challenges for immunotherapy when such mutations are present. Recent studies have expanded the understanding of the relationship between immunotherapy and IRF8. In the tumor environment, the SHP-2 and PD-1-SHP-2 axis inhibits the

differentiation of the monocyte/DC lineage by affecting IRF8 phosphorylation, thereby impairing monocyte and DC development and neutrophil differentiation[44]. This disruption in the myeloid cell landscape weakens the body's anti-tumor immune capacity. These findings provide further evidence for IRF8's role in immunotherapy, opening new avenues for exploring its mechanisms and applications. They support investigating IRF8's potential in cancer immunotherapy and aid in optimizing treatment strategies.

Notably, there have been no reports on IRF8 as a predictive indicator of immunotherapy efficacy in solid tumors. This study is the first to associate IRF8 expression levels with anti-PD-1 treatment efficacy in LUAD. Additionally, our cohort was among the first to conduct a retrospective prognostic analysis on predictive indicators of anti-PD-1 treatment efficacy in first-line treatment of inoperable NSCLC. We believe these findings offer valuable insights for clinical decision-making.

This study has several limitations related to sample size. The immunotherapy cohort comprised only 44 patients, with subgroup analyses of combination chemotherapy regimens (pemetrexed plus platinum [PP] or paclitaxel plus cisplatin [TP]) further constrained by reduced statistical power. Notably, the limited representation of individual PD-1 inhibitors precluded robust comparisons of inter-agent efficacy. These constraints underscore the need for validation in expanded cohorts incorporating diverse therapeutic combinations. Furthermore, prospective multicenter studies are warranted to determine whether IRF8 exhibits class-agnostic predictive utility across PD-1/PD-L1 blockade agents.

Conclusions

Identifying biomarkers that effectively predict ICI's efficacy is currently a challenging area in clinical research. So far, over 40 predictive biomarkers are under evaluation, but there is no consensus on which one is most promising. In this retrospective study, IRF8 expression was associated with enhanced immune cell infiltration and improved immunotherapy response in LUAD. They might serve as markers for prognostication and the effectiveness of immunotherapy in LUAD patients. However, our study has some limitations. First, in our IHC cohort, some tissues were obtained from biopsies, which might not provide a comprehensive view of the tumor microenvironment due to the small tissue size. This could lead to biased results. Moreover, only 44 LUAD patients were treated with anti-PD-1 therapy. This small sample size may limit the generalizability of our findings. Moreover, the role of IRF8 in promoting alterations within the tumor microenvironment (TME) of lung adenocarcinoma lacks experimental verification, especially regarding how IRF8 induces the suppression of CD8 + T cells and the recruitment of tumor-associated macrophages. Hence, our current findings merely provide theoretical perspectives. Future studies should prioritize functional experiments (e.g., immune-competent murine models, in vitro co-culture systems) to elucidate whether IRF8 directly modulates immune evasion or merely correlates with these phenotypes. To validate our findings, further clinical trials and basic experiments are needed to elucidate the specific mechanism of action of this phenotype.

Data availability

All data generated or analysed during this study are included in this published article (and its Supplementary Information files).

Received: 6 November 2024; Accepted: 13 March 2025
Published online: 20 March 2025

References

1. Sung, H. et al. Global cancer statistics 2020: GLOBOCAN estimates of incidence and mortality worldwide for 36 cancers in 185 countries. *CA Cancer J. Clin.* **71**(3), 209–249 (2021).
2. Ribas, A. & Wolchok, J. D. Cancer immunotherapy using checkpoint blockade. *Science* **359**(6382), 1350–1355 (2018).
3. Garcia-Diaz, A. et al. Interferon receptor signaling pathways regulating PD-L1 and PD-L2 expression. *Cell. Rep.* **19**(6), 1189–1201 (2017).
4. Negishi, H., Taniguchi, T. & Yanai, H. The interferon (IFN) class of cytokines and the IFN regulatory factor (IRF) transcription factor family. *Cold Spring Harb. Perspect. Biol.* **10**(11), e028423 (2018).
5. Kawai, T. et al. Interferon-alpha induction through Toll-like receptors involves a direct interaction of IRF7 with MyD88 and TRAF6. *Nat. Immunol.* **5**(10), 1061–1068 (2004).
6. Yasuda, K. et al. Phenotype and function of B cells and dendritic cells from interferon regulatory factor 5-deficient mice with and without a mutation in DOCK2. *Int. Immunol.* **25**(5), 295–306 (2013).
7. Lazear, H. M., Nice, T. J. & Diamond, M. S. Interferon-lambda: Immune functions at barrier surfaces and beyond. *Immunity* **43**(1), 15–28 (2015).
8. Sun, L. et al. Cyclic GMP-AMP synthase is a cytosolic DNA sensor that activates the type I interferon pathway. *Science* **339**(6121), 786–791 (2013).
9. Tamura, T. et al. The IRF family transcription factors in immunity and oncogenesis. *Annu. Rev. Immunol.* **26**, 535–584 (2008).
10. Odendall, C. et al. Diverse intracellular pathogens activate type III interferon expression from peroxisomes. *Nat. Immunol.* **15**(8), 717–726 (2014).
11. Kovács, S. A., Fekete, J. T. & Győrffy, B. Predictive biomarkers of immunotherapy response with pharmacological applications in solid tumors. *Acta Pharmacol. Sin.* **44**(9), 1879–1889 (2023).
12. Eddy, J. A. et al. CRI iAtlas: An interactive portal for immuno-oncology research. *F1000Res.* **9**, 1028 (2020).
13. Li, T. et al. TIMER2.0 for analysis of tumour-infiltrating immune cells. *Nucleic Acids Res.* **48**(W1), W509–W514 (2020).
14. Hanzelmann, S., Castelo, R. & Guinney, J. GSVA: Gene set variation analysis for microarray and RNA-seq data. *BMC Bioinform.* **14**, 7 (2013).
15. Sun, D. et al. TISCH: A comprehensive web resource enabling interactive single-cell transcriptome visualization of tumor microenvironment. *Nucleic Acids Res.* **49**(D1), D1420–D1430 (2021).
16. Ru, B. et al. TISIDB: An integrated repository portal for tumour-immune system interactions. *Bioinformatics* **35**(20), 4200–4202 (2019).
17. Reck, M. et al. Pembrolizumab versus chemotherapy for PD-L1-positive non-small-cell lung cancer. *N. EnglJ. Med.* **375**(19), 1823–1833 (2016).

18. Langer, C. J. et al. Carboplatin and pemetrexed with or without pembrolizumab for advanced, non-squamous non-small-cell lung cancer: A randomised, phase 2 cohort of the open-label KEYNOTE-021 study. *Lancet Oncol.* **17**(11), 1497–1508 (2016).
19. Antonia, S. J. et al. Durvalumab after chemoradiotherapy in stage III non-small-cell lung cancer. *N. EnglJ. Med.* **377**(20), 1919–1929 (2017).
20. Sharma, P. et al. Primary, adaptive, and acquired resistance to cancer immunotherapy. *Cell* **168**(4), 707–723 (2017).
21. Klement, J. D. et al. Tumor PD-L1 engages myeloid PD-1 to suppress type I interferon to impair cytotoxic T lymphocyte recruitment. *Cancer Cell.* **41**(3), 620-636.e9 (2023).
22. Garris, C. S. et al. Successful Anti-PD-1 cancer immunotherapy requires t cell-dendritic cell crosstalk involving the cytokines IFN-γ and IL-12. *Immunity* **55**(9), 1749. https://doi.org/10.1016/j.immuni.2022.07.021 (2022).
23. Gao, J. et al. Loss of IFN-gamma pathway genes in tumor cells as a mechanism of resistance to anti-CTLA-4 therapy. *Cell* **167**(2), 397-404.e9 (2016).
24. Woods, H. et al. Computational modeling and prediction of deletion mutants. *Structure* **31**(6), 713-723.e3 (2023).
25. Burchert, A. et al. Interferon consensus sequence binding protein (ICSBP; IRF-8) antagonizes BCR/ABL and down-regulates bcl-2. *Blood* **103**(9), 3480–3489 (2004).
26. Murakami, K. et al. A RUNX-CBFbeta-driven enhancer directs the IRF8 dose-dependent lineage choice between DCs and monocytes. *Nat. Immunol.* **22**(3), 301–311 (2021).
27. Kurotaki, D. et al. IRF8 inhibits C/EBPalpha activity to restrain mononuclear phagocyte progenitors from differentiating into neutrophils. *Nat. Commun.* **5**, 4978 (2014).
28. Bovolenta, C. et al. Molecular interactions between interferon consensus sequence binding protein and members of the interferon regulatory factor family. *Proc. Natl. Acad. Sci. USA* **91**(11), 5046–5050 (1994).
29. Nelson, N. et al. Interferon consensus sequence-binding protein, a member of the interferon regulatory factor family, suppresses interferon-induced gene transcription. *Mol. Cell Biol.* **13**(1), 588–599 (1993).
30. Wu, H. et al. Hepatic interferon regulatory factor 8 expression suppresses hepatocellular carcinoma progression and enhances the response to anti-programmed cell death protein-1 therapy. *Hepatology* **76**(6), 1602–1616 (2022).
31. Gatti, G. et al. High IRF8 expression correlates with CD8 T cell infiltration and is a predictive biomarker of therapy respons in ER-negative breast cancer. *Breast Cancer Res.* **23**(1), 40 (2021).
32. Qiu Z, Khalife J, Ethiraj P, et al. IRF8-mutant B cell lymphoma evades immunity through a CD74-dependent deregulation of antigen processing and presentation in MHCII complexes. Sci Adv. 2024;10(28): eadk2091.
33. Cytlak, U. et al. Differential IRF8 transcription factor requirement defines two pathways of dendritic cell development in humans. *Immunity* **53**(2), 353-370.e8 (2020).
34. Kim, S. et al. High amount of transcription factor IRF8 engages AP1-IRF composite elements in enhancers to direct type 1 conventional dendritic cell identity. *Immunity* **53**(4), 759-774.e9 (2020).
35. Ascic, E. et al. In vivo dendritic cell reprogramming for cancer immunotherapy. *Science* **386**(6719), eadn9083 (2024).
36. Zimmermannova, O. et al. Restoring tumor immunogenicity with dendritic cell reprogramming. *Sci. Immunol.* **8**(85), eadd4817 (2023).
37. Durai, V. et al. Cryptic activation of an Irf8 enhancer governs cDC1 fate specification. *Nat. Immunol.* **20**(9), 1161–1173 (2019).
38. Vander, H. M., Cantley, L. C. & Thompson, C. B. Understanding the Warburg effect: The metabolic requirements of cell proliferation. *Science* **324**(5930), 1029–1033 (2009).
39. Kurniawan, H. et al. Glutathione restricts serine metabolism to preserve regulatory T cell function. *Cell Metab.* **31**(5), 920-936.e7 (2020).
40. Zhou, Y. et al. Silencing of IRF8 mediated by m6A modification promotes the progression of T-cell acute lymphoblastic leukemia. *Adv. Sci. (Weinh).* **10**(2), e2201724. https://doi.org/10.1002/advs.202201724 (2023).
41. He, Y., Jiang, Z., Chen, C. & Wang, X. Classification of triple-negative breast cancers based on Immunogenomic profiling. *J. Exp. Clin. Cancer Res.* **37**(1), 327 (2018).
42. Tse, B. C. Y. et al. CD11c+ and IRF8+ cell densities in rectal cancer biopsies predict outcomes of neoadjuvant chemoradiotherapy. *Oncoimmunology* **12**(1), 2238506 (2023).
43. Sworder, B. J. et al. Determinants of resistance to engineered T cell therapies targeting CD19 in large B cell lymphomas. *Cancer Cell* **41**(1), 210-225.e5 (2023).
44. Christofides, A. et al. SHP-2 and PD-1-SHP-2 signaling regulate myeloid cell differentiation and antitumor responses. *Nat. Immunol.* **24**(1), 55–68 (2023).

Acknowledgements

The authors are grateful for the helpful editors and reviewers' comments on this paper. Special thanks to Dr.Baoqing Tian, Dr.Xiaozheng Chen, and Dr.You Mo for their assistance during the revision process of this article.

Author contributions

Wen Huo: Data analysis and Writing, Conceptualization. Minxin Chen: Formal analysis, Software, Conceptualization. Cheng Chang: Validation, Resources, Investigation. Jinming Yu: Project Administration and Contributed Significantly to Analysis and Manuscript Preparation. Dawei Chen: Conceptualization, Project Administration, Manuscript Review and Editing. Ruozheng Wang: Project Administration, Manuscript Review and Financial Support for the Project.

Funding

This study was funded by the Science and Technology Assistance Project of the Science and Technology Department of the Autonomous region(2022E02050), Project of the Central Government guiding Local Science and Technology (ZYYD2022B18).

Declarations

Competing interests

The authors declare no competing interests.

Additional information

Supplementary Information The online version contains supplementary material available at https://doi.org/10.1038/s41598-025-94424-0.

Correspondence and requests for materials should be addressed to J.Y., D.C. or R.W.